Preparation and Characterization of the Eu^{3+} Doped Perovskite Nanosheet Phosphor: $La_{0.90}Eu_{0.05}Nb_2O_7$

Tadashi C. Ozawa,* Katsutoshi Fukuda, Kosho Akatsuka, Yasuo Ebina, and Takayoshi Sasaki

Nanoscale Materials Center, National Institute for Materials Science, 1-1 Namiki, Tsukuba, Ibaraki, 305-0044, Japan

Received September 7, 2007. Revised Manuscript Received November 1, 2007

Eu^{3+}-doped perovskite nanosheets, $La_{0.90}Eu_{0.05}Nb_2O_7$, have been prepared by the soft chemical exfoliation reaction of $K_{1-x}H_xLa_{0.90}Eu_{0.05}Nb_2O_7$ with a tetrabuthylammonium hydroxide aqueous solution. The resulting colloidal $La_{0.90}Eu_{0.05}Nb_2O_7$ nanosheet suspension exhibits photoluminescence emission from the $^5D_0$ to ^7F_J manifold transitions of Eu^{3+} by either direct excitation of Eu^{3+} or host excitation, whereas no host emission was observed at room temperature. In the case of the bulk precursors $K_{1-x}H_xLa_{0.90}Eu_{0.05}Nb_2O_7$, the direct excitation yields more intense emission than the host excitation. On the contrary, the most intense emission from the $La_{0.90}Eu_{0.05}Nb_2O_7$ nanosheets was observed by exciting at the broad excitation band maximum (353 nm). The difference in the photoluminescence properties between the $La_{0.90}Eu_{0.05}Nb_2O_7$ nanosheets and their bulk precursors seems to be related to the dimensionality of these host structures and the confinement of the energy-transfer process between the host layer units and Eu^{3+} activators.

Introduction

In recent years, several studies on photoluminescence properties of nanosheets and related materials have been reported.[1–8] These nanosheet-based phosphors are quite intriguing because photoluminescence excitation energy is more effectively absorbed when the surface area is large, and nanosheets have a considerably large surface-to-volume ratio with respect to those of bulk materials. Furthermore, the morphology of nanosheets is suitable for fabricating optoelectronic devices such as electroluminescence panels, which consist of a stack of functional layers or sheets.[9] The majority of nanosheet-based phosphor materials reported to date can be categorized into two groups. In one group, nanosheets themselves exhibit photoluminescence. Among those, blue photoluminescence reported for $Ti_{0.91}O_2$,[1] surface-oxidized Si,[7] and Bi−Sr−Ta−O nanosheets[8] are of particular importance for technological applications. In the other group, phosphors are composed by insertion of photoactive components such as Ln (lanthanide) ions or Ln-containing complexes between transition metal oxide nanosheets.[2–6]

In the studies of the latter group, nanosheet-based phosphors, effective energy transfer from the transition metal oxide nanosheet hosts to Ln luminescence activators was observed. Many of the practical phosphors contain Ln activators because of their high emission intensities and well-predictable emission wavelengths from the intra-4f transitions. Therefore, utilization of energy transfer from the transition metal oxide nanosheets to Ln activators seems a feasible approach to design practical phosphors.

However, photoluminescence properties of Ln intercalated nanosheets tend to be quite susceptible to the amount of cointercalated species, such as H_2O and hydronium ions, which act as energy-transfer mediators.[4–6] Because the amount of these energy-transfer mediators depends on temperature, thermal stabilities of these nanosheet-based phosphors would be a critical issue. In addition, when considering the energy-transfer probabilities in phosphor materials, strength of the interaction between hosts and activators is one of the crucial factors. By considering these aspects, it seems rational to expect that if activators are incorporated in intrananosheet sites rather than in inter-nanosheet sites, the stabilities of photoluminescence properties and efficiency of energy transfer from the host units to the activators might significantly be improved. One of the candidate host nanosheets for such an ideal phosphor material is $LaNb_2O_7$ nanosheet. This perovskite type nanosheet can be obtained by protonation of $KLaNb_2O_7$ followed by soft chemical exfoliation of the protonated phase using a tetrabuthylammonium hydroxide (TBA^+OH^-) aqueous solu-

* To whom correspondence should be addressed. E-mail: OZAWA.Tadashi@nims.go.jp.

(1) Sasaki, T.; Watanabe, M. *J. Phys. Chem. B* **1997**, *101*, 10159.
(2) Xin, H.; Ma, R.; Wang, L.; Ebina, Y.; Takada, K.; Sasaki, T. *Appl. Phys. Lett.* **2004**, *85*, 4187.
(3) Xin, H.; Ebina, Y.; Ma, R.; Takada, K.; Sasaki, T. *J. Phys. Chem. B* **2006**, *110*, 9863.
(4) Matsumoto, Y.; Unal, U.; Kimura, Y.; Ohashi, S.; Izawa, K. *J. Phys. Chem. B* **2005**, *109*, 12748.
(5) Ida, S.; Unal, U.; Izawa, K.; Altuntasoglu, O.; Ogata, C.; Inoue, T.; Shimogawa, K.; Matsumoto, Y. *J. Phys. Chem. B* **2006**, *110*, 23881.
(6) Ida, S.; Araki, K.; Unal, U.; Izawa, K.; Altuntasoglu, O.; Ogata, C.; Matsumoto, Y. *Chem. Commun.* **2006**, 3619.
(7) Nakano, H.; Mitsuoka, T.; Harada, M.; Horibuchi, K.; Nozaki, H.; Takahashi, N.; Nonaka, T.; Seno, Y.; Nakamura, H. *Angew. Chem., Int. Ed.* **2006**, *45*, 6303.
(8) Ida, S.; Ogata, C.; Unal, U.; Izawa, K.; Inoue, T.; Altuntasoglu, O.; Matsumoto, Y. *J. Am. Chem. Soc.* **2007**, *129*, 8956.
(9) Frey, G. L.; Reynolds, K. J.; Friend, R. H. *Adv. Mater.* **2002**, *14*, 265.

10.1021/cm702552p CCC: $37.00
Published on Web 11/27/2007

tion.[10] In addition, room-temperature photoluminescence from the Eu^{3+}-doped $KLaNb_2O_7$ bulk sample has already been confirmed.[11] Among various Ln activators, Eu^{3+} is of particular interest because of its strong and well-defined red photoluminescence property. Therefore, it would be quite worthwhile to investigate the photoluminescence property of Eu^{3+}-doped $LaNb_2O_7$ nanosheets and to compare it with those of the bulk precursors $K_{1-x}H_xLaNb_2O_7/Eu^{3+}$. Furthermore, the Eu^{3+}-doped $LaNb_2O_7$ nanosheets might be an ideal phosphor for the new generation solid-state lighting based on GaN. The 2% Eu^{3+} doped $KLaNb_2O_7$ bulk sample has an absorption edge around 370 nm,[11] whereas the GaN-based solid-state lighting requires phosphors that can effectively be excited in the near-UV range (350–400 nm).[12,13] Thus, if more efficient energy transfer from the host to the activators could be induced by exfoliating bulk $KLaNb_2O_7/Eu^{3+}$ into $LaNb_2O_7/Eu^{3+}$ nanosheets, the application of these nanosheets to the phosphors for solid-state lighting seems feasible.

In the early stage of our investigation, we attempted to prepare stoichiometric nanosheets of $LaNb_2O_7/Eu^{3+}$. However, the single-phase stoichiometric bulk precursor $KLaNb_2O_7/Eu^{3+}$ could not be synthesized. As reported by Sato et al., the starting component amount for Ln had to be reduced slightly in order to obtain single-phase $KLn_{1-\delta}Nb_2O_7$.[14] In this paper, we report the results of preparation, in-plane X-ray diffraction, AFM imaging, UV–vis absorption and diffuse reflection spectroscopy, and photoluminescence excitation and emission property characterizations of $La_{0.90}Eu_{0.05}Nb_2O_7$ nanosheets. In addition, the comparison of the properties among the $La_{0.90}Eu_{0.05}Nb_2O_7$ nanosheets, their bulk precursors, and other related Eu^{3+}-doped oxide phosphors will be discussed.

Experimental Section

Materials. $La_{0.90}Eu_{0.05}Nb_2O_7$ nanosheets were prepared in three step reactions as schematically shown in Figure 1. The first precursor $KLa_{0.90}Eu_{0.05}Nb_2O_7$ was prepared by the previously reported method for the undoped phase $KLaNb_2O_7$[14,15] with a slight modification. The starting components K_2CO_3 and Nb_2O_5 were used as received, and La_2O_3 and Eu_2O_3 were dried at 800 °C before use. As reported by Sato et al.,[14] the staring component amount of Ln_2O_3 (Ln = La or Eu) had to be reduced from the stoichiometric one for $KLnNb_2O_7$ in order to avoid the coproduction of impurity phases like $LnNbO_4$.[16] In case of 5% Eu^{3+} doping, 5% reduction of *Ln* was necessary to obtain the single-phase precursor $KLa_{0.90}Eu_{0.05}Nb_2O_7$. Furthermore, a 15% excess of K_2CO_3 was used in order to compensate for its loss by evaporation during the heating reaction. The starting materials of 1.15:0.90:0.05:2.00 K_2CO_3:La_2O_3:Eu_2O_3:Nb_2O_5 were mixed thoroughly in an agate mortar, and the resulting mixture was pressed into a pellet, placed on an alumina boat, heated at 1150 °C for 1 h, and furnace-cooled.

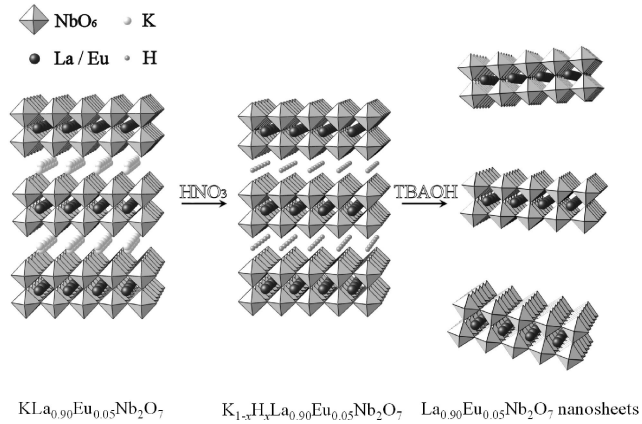

Figure 1. Schematic drawing of the three-step $La_{0.90}Eu_{0.05}Nb_2O_7$ nanosheet preparation reactions. Only half of the K^+ site is occupied in $KLa_{0.90}Eu_{0.05}Nb_2O_7$.

The second step was an ion-exchange reaction of K^+ in $KLa_{0.90}Eu_{0.05}Nb_2O_7$ with H^+. 1.5 g of $KLa_{0.90}Eu_{0.05}Nb_2O_7$ product was ground into powder and reacted with 50 mL of 10 M HNO_3 for 3 days at room temperature under vigorous shaking. The protonated precursor was isolated by filtration and washed with water.

Finally, $La_{0.90}Eu_{0.05}Nb_2O_7$ nanosheets were obtained by a method similar to that reported for undoped $LaNb_2O_7$ nanosheets.[10] One gram of protonated precursor $K_xH_{1-x}La_{0.90}Eu_{0.05}Nb_2O_7$ was vigorously shaken with 250 mL of a 5-fold excess ($TBA^+/H^+ = 5$) TBAOH aqueous solution for 1 week. The resulting $La_{0.90}Eu_{0.05}Nb_2O_7$ nanosheet suspension was then isolated from the unreacted residue by centrifugation.

Characterization. The phase purity of precursors was examined by powder X-ray diffraction using Cu *K*α radiation on a Rigaku RINT2200V/PC diffractometer. The elemental composition of the protonated precursor was characterized by ICP-AES on a Seiko Instruments SPS1700HVR spectrometer. Completion of the protonation reaction and the hydration amount of the protonated precursor were examined by thermogravimetric analysis (TGA) on a Rigaku Thermo Plus TG 8120 at a rate of 1 °C/min up to 1000 °C. The tapping-mode AFM image of $La_{0.90}Eu_{0.05}Nb_2O_7$ nanosheets, which were electrostatically deposited[17] on a Si substrate, was obtained using a Seiko Instruments SPA-400 AFM system with a Si tip cantilever (20 N m^{-1}) in the DFM mode. The crystallinity of the nanosheets, deposited on a Si substrate by the Langmuir–Blodgett (LB) method,[18] was characterized by in-plane X-ray diffraction using synchrotron radiation ($\lambda = 0.11966(4)$ nm) of the Photon Factory BL-3A at High Energy Accelerator Research Organization (KEK). The UV–vis spectra of the nanosheet suspension were measured on a HITACHI U-4100 spectrometer. The diffuse reflection spectra of the bulk precursors were measured using a HITACHI U-4000 spectrometer, and the reflection spectra were converted to the absorbance spectra by the Kubelka–Munk method. Finally, photoluminescence excitation and emission spectra were measured on a Hitachi F-4500 fluorescence spectrophotometer at room temperature. The excitation spectra were corrected for the spectral distribution of the lamp intensity by the Rhodamine B method, and the emission spectra were corrected for the spectral response of the instrument using a substandard light source.

(10) Schaak, R. E.; Mallouk, T. E. *Chem. Mater.* **2000**, *12*, 2513.
(11) Kudo, A. *Chem. Mater.* **1997**, *9*, 664.
(12) Neeraj, S.; Kijima, N.; Cheetham, A. K. *Solid State Commun.* **2004**, *131*, 65.
(13) Neeraj, S.; Kijima, N.; Cheetham, A. K. *Chem. Phys. Lett.* **2004**, *387*, 2.
(14) Sato, M.; Abo, J.; Jin, T.; Ohta, M. *Solid State Ionics* **1992**, *51*, 85.
(15) Kobayashi, Y.; Schottenfeld, J. A.; Macdonald, D. D.; Mallouk, T. E. *J. Phys. Chem. C* **2007**, *111*, 3185.
(16) Toda, K.; Honda, M.; Ishimoto, Y.; Ye, Z.-G.; Sato, M. *Solid State Ionics* **2000**, *136*, 25.
(17) Wang, L.; Sasaki, T.; Ebina, Y.; Kurashima, K.; Watanabe, M. *Chem. Mater.* **2002**, *14*, 4827.
(18) Muramatsu, M.; Akatsuka, K.; Ebina, Y.; Wang, K.; Sasaki, T.; Ishida, T.; Miyake, K.; Haga, M. *Langmuir* **2005**, *21*, 6590.

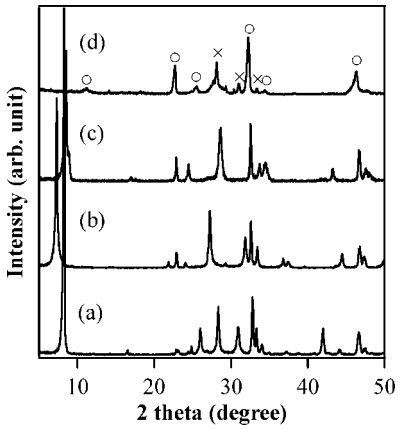

Figure 2. Powder X-ray diffraction profiles of (a) $KLa_{0.90}Eu_{0.05}Nb_2O_7$, (b) $K_{0.08}H_{0.92}La_{0.90}Eu_{0.05}Nb_2O_7 \cdot 0.25H_2O$ dried at room temperature, (c) $K_{0.08}H_{0.92}La_{0.90}Eu_{0.05}Nb_2O_7$ dried at 200 °C, and (d) $K_{0.08}H_{0.92}La_{0.90}Eu_{0.05}Nb_2O_7$ after TGA up to 1000 °C. Symbols ○ and × indicate expected diffraction peak positions of $Ln_{1/3-\delta}NbO_3$ and $LnNbO_4$ (Ln = La or Eu), respectively.

Table 1. Lattice Parameters of $KLa_{0.90}Eu_{0.05}Nb_2O_7$, $KLaNb_2O_7$, and Their Protonated Forms

	a (nm)	*b* (nm)	*c* (nm)
$KLa_{0.90}Eu_{0.05}Nb_2O_7$	0.3904(1)	2.1490(6)	0.3877(1)
$KLaNb_2O_7$ [a]	0.39060(1)	2.16030(7)	0.38879(1)
$K_{0.08}H_{0.92}La_{0.90}Eu_{0.05}Nb_2O_7 \cdot 0.25H_2O$ at RT	0.3885(9)	$a = b$	1.2194(3)
$HLaNb_2O_7 \cdot xH_2O$ at RT[b]	0.3891(2)	$a = b$	1.2213(6)
$K_{0.08}H_{0.92}La_{0.90}Eu_{0.05}Nb_2O_7$ at 200 °C	0.38842(9)	$a = b$	1.0438(3)
$HLaNb_2O_7 \cdot xH_2O$ at 200 °C[b]	0.3894(3)	$a = b$	1.0459(7)

[a] See ref 14. [b] See ref 19.

Results and Discussions

The powder X-ray diffraction patterns of the precursors $KLa_{0.90}Eu_{0.05}Nb_2O_7$ and $K_{1-x}H_xLa_{0.90}Eu_{0.05}Nb_2O_7 \cdot yH_2O$ are shown in Figure 2a−c. The diffraction patterns of these precursors agree well with those of the previously reported undoped phases.[14,19–23] The refined lattice parameters of the Eu^{3+}-doped and previously reported undoped bulk phases are summarized in Table 1. All these phases are $n = 2$ members of the Dion−Jacobson type layered perovskites $A[M_{n-1}B_nO_{3n+1}]$.[24,25] The orthorhombic unit cells of the K phases contain four Nb−O octahedra layers along the *b*-axis, and the lattice parameters *a* and *c* correspond to the intralayer Nb−O−Nb distances. On the other hand, the tetragonal unit cells of the protonated phases contain two Nb−O octahedra layers along the *c*-axis, and the lattice parameters *a* (= *b*) correspond to the intralayer Nb−O−Nb distances. Overall, intralayer Nb−O−Nb and intralayer distances of the Eu^{3+}-doped phases in this study are slightly smaller than those of the undoped phases, reflecting the smaller ionic radius of Eu^{3+} than La^{3+} and/or slight deficiency in the Ln^{3+} site. In addition, the protonated phases dried at room temperature have larger lattice parameters than the others along the interlayer direction because of their significant hydration, which is confirmed by TGA as described later.

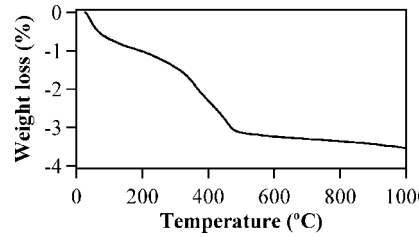

Figure 3. Thermogravimetric analysis result of the protonated precursor, $H_{0.92}K_{0.08}La_{0.90}Eu_{0.05}Nb_2O_7 \cdot 0.25H_2O$.

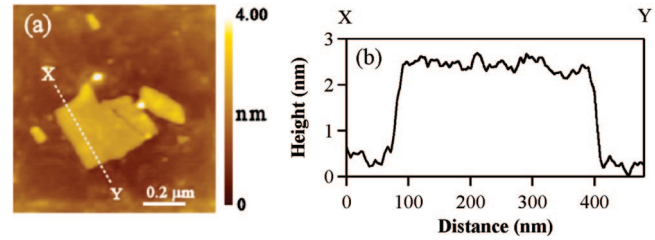

Figure 4. (a) AFM image and (b) cross-sectional profile of $La_{0.90}Eu_{0.05}Nb_2O_7$ nanosheets.

The ICP-AES analysis result for the protonated precursor indicates that its composition is 0.08:0.89:0.05:2.00 K:La:Eu:Nb. The contents of La, Eu, and Nb are identical to the nominal composition within the experimental uncertainties, suggesting no decomposition of the parent layer unit $La_{0.90}Eu_{0.05}Nb_2O_7$ during the protonation reaction. The protonation reaction was close to complete as indicated by the significantly reduced K content, but a small portion of K was left unreacted. The experimentally estimated formula of the protonated precursor in this study is $K_{0.08}H_{0.92}La_{0.90}Eu_{0.05}Nb_2O_7$. Various other protonation reaction conditions have also been tested, but no lower K^+ content precursor was obtained.

The TGA result for the protonated precursor is shown in Figure 3. The intercalated H_2O was dehydrated below 200 °C. The hydration amount of the room-temperature-dried protonated precursor estimated from the analysis is 0.25 mol of H_2O per 1 mol of $K_{0.08}H_{0.92}La_{0.90}Eu_{0.05}Nb_2O_7$. The powder X-ray diffraction pattern of the sample heated up to 1000 °C is shown in Figure 2d. The protonated precursor was decomposed into $Ln_{1/3-\delta}NbO_3$ and $LnNbO_4$ at high temperature. This result is consistent with the weight loss due to deprotonation observed in the TGA between 200 and 500 °C.

The protonated precursor was successfully exfoliated into $La_{0.90}Eu_{0.05}Nb_2O_7$ nanosheets by reacting it with a TBAOH aqueous solution. Figure 4a shows a topographic image of the $La_{0.90}Eu_{0.05}Nb_2O_7$ nanosheet deposited on a Si substrate using polyethylenimine (PEI) as an electrostatic glue layer.[26,27]

(19) Gopalakrishnan, J.; Bhat, V.; Raveau, B. *Mater. Res. Bull.* **1987**, *22*, 413.
(20) Suzuki, H.; Notsu, K.; Takeda, Y.; Sugimoto, W.; Sugahara, Y. *Chem. Mater.* **2003**, *15*, 636.
(21) Matsuda, T.; Fujita, T.; Miyamae, N.; Takeuchi, M.; Kanda, K. *Bull. Chem. Soc. Jpn.* **1993**, *66*, 1548.
(22) Takeda, Y.; Suzuki, H.; Notsu, K.; Sugimoto, W.; Sugahara, Y. *Mater. Res. Bull.* **2006**, *41*, 834.
(23) Sato, M.; Abo, J.; Jin, T.; Ohta, M. *J. Alloys Compd.* **1993**, *192*, 81.
(24) Dion, M.; Ganne, M.; Tournoux, M. *Mater. Res. Bull.* **1981**, *16*, 1429.
(25) Jacobson, A. J.; Johnson, J. W.; Lewandowski, J. T. *Inorg. Chem.* **1985**, *24*, 3727.
(26) Sasaki, T.; Ebina, Y.; Watanabe, M.; Decher, G. *Chem. Commun.* **2000**, 2163.
(27) Fukuda, K.; Nakai, I.; Ebina, Y.; Tanaka, M.; Mori, T.; Sasaki, T. *J. Phys. Chem. B* **2006**, *110*, 17070.

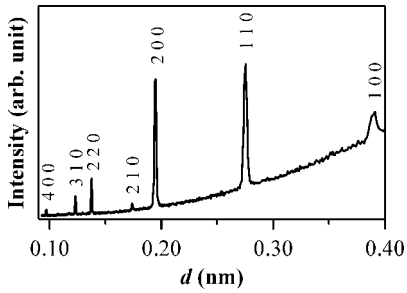

Figure 5. In-plane X-ray diffraction profile of $La_{0.90}Eu_{0.05}Nb_2O_7$ nanosheets.

The $La_{0.90}Eu_{0.05}Nb_2O_7$ nanosheet product has an approximate mean lateral size of 0.4 μm, and the thickness is uniformly 2.01(1) nm. This thickness is larger than that of the single $La_{0.90}Eu_{0.05}Nb_2O_7$ layer (1.06 nm) estimated from the crystallographic data. The thickness of many other oxide nanosheets observed by AFM is also larger than that estimated by the crystallographic data because of absorption of oxonium and TBA^+ ions, and other uncertain factors.[6,27–33] In this sense, our $La_{0.90}Eu_{0.05}Nb_2O_7$ nanosheets are fairly likely to be homogeneously unilamellar.

The result of the in-plane X-ray diffraction for $La_{0.90}Eu_{0.05}Nb_2O_7$ nanosheets deposited on a Si substrate is shown in Figure 5. All the observed reflections can be indexed to *h k* 0 of the precursor layered perovskite structure.[14] The refined lattice parameter ($a = b = 0.3912(6)$ nm) of the nanosheets corresponds well to those of the bulk precursor phases (Table 1) indicating that the exfoliated nanosheets are crystalline and retain the layered perovskite structural feature of the precursors.

The UV–vis absorption spectra of the diluted nanosheet suspension are shown in Figure 6. The $La_{0.90}Eu_{0.05}Nb_2O_7$ nanosheets exhibit broad optical absorption peaks with the maxima at 232 and 316 nm, and their extinction coefficients are 2.2×10^4 and 2.0×10^3 dm^3 mol^{-1} cm^{-1}, respectively. In addition, a shoulder was observed around 270 nm in the absorption spectra. Similar absorption characteristics was observed for titania nanosheet, and those are attributed to the band gap of the titania nanosheet itself and the interference effect among the nanosheets.[34] Thus, the absorption features in this study could also be attributed to the same origin. The comparison between the UV–vis absorption spectrum of $La_{0.90}Eu_{0.05}Nb_2O_7$ nanosheets and diffuse reflection spectra of $K_{1-x}H_xLa_{0.90}Eu_{0.05}Nb_2O_7$ precursors is shown in Figure 7. The absorption edge of $La_{0.90}Eu_{0.05}Nb_2O_7$ nanosheets was observed at 347 nm, which is blue-shifted with respect to those of the bulk precursors $KLa_{0.90}Eu_{0.05}Nb_2O_7$

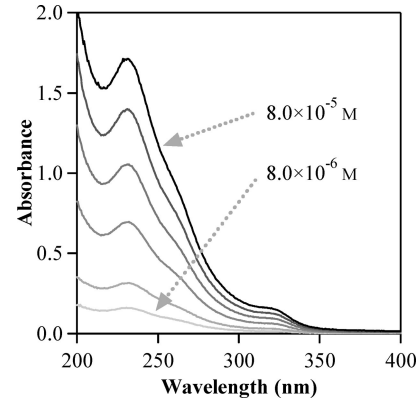

Figure 6. UV–vis absorption spectra of the $La_{0.90}Eu_{0.05}Nb_2O_7$ nanosheet suspension. The absorbance increases linearly as the concentration of the nanosheets increases as 8.0×10^{-6} (lightest gray line), 1.6×10^{-5}, 3.2×10^{-5}, 4.8×10^{-5}, 6.4×10^{-5}, and 8.0×10^{-5} M (black line).

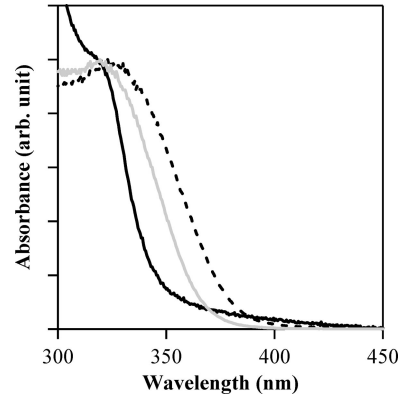

Figure 7. Diffuse reflection spectra of $KLa_{0.90}Eu_{0.05}Nb_2O_7$ (gray solid line), $H_{0.98}K_{0.08}La_{0.90}Eu_{0.05}Nb_2O_7 \cdot 0.25H_2O$ (black dotted line), and absorption spectrum of $La_{0.90}Eu_{0.05}Nb_2O_7$ nanosheets (black solid line).

and $K_{0.08}H_{0.92}La_{0.90}Eu_{0.05}Nb_2O_7 \cdot 0.25H_2O$, whose absorption edges are at 366 and 380 nm, respectively. Similar blue shifts of the absorption edges were commonly observed in other oxide nanosheets with respect to those of their bulk precursors.[1,33,34] By considering the quantum size effect driven blue shift in these previously reported nanosheets and many other nanomaterials, the blue shift in the $La_{0.90}Eu_{0.05}Nb_2O_7$ nanosheets probably has the same origin.

The photoluminescence excitation and emission spectra of the bulk precursors and exfoliated $La_{0.90}Eu_{0.05}Nb_2O_7$ nanosheets are shown in Figures 8 and 9, respectively. For all these phases, sharp emission from the lowest excited state $^5D_0$ to ^7F_J manifold transitions of Eu^{3+} was observed, whereas no host luminescence was observed at room temperature. The highest emission intensity observed for all these phases is from the hypersensitive forced electric dipole $^5D_0 \rightarrow {}^7F_2$ transition of Eu^{3+}. The fact that the dominant emission is from the parity forbidden electric dipole transition rather than from the magnetic dipole transition ($^5D_0 \rightarrow {}^7F_1$) indicates that Eu^{3+} is located at the site with no inversion symmetry in all these phases.[4,35,36]

For both bulk precursors and $La_{0.90}Eu_{0.05}Nb_2O_7$ nanosheets, no emission was observed when the excitation wavelength

(28) Sasaki, T.; Ebina, Y.; Kitami, Y.; Watanabe, M.; Oikawa, T. *J. Phys. Chem. B* **2001**, *105*, 6116.
(29) Fukuda, K.; Ebina, Y.; Shibata, T.; Aizawa, T.; Nakai, I.; Sasaki, T. *J. Am. Chem. Soc.* **2007**, *129*, 202.
(30) Omomo, Y.; Sasaki, T.; Wang, L.; Watanabe, M. *J. Am. Chem. Soc.* **2003**, *125*, 3568.
(31) Ma, R.; Liu, Z.; Li, L.; Iyi, N.; Sasaki, T. *J. Mater. Chem.* **2006**, *16*, 3809.
(32) Liu, Z.; Ma, R.; Osada, M.; Iyi, N.; Ebina, Y.; Takada, K.; Sasaki, T. *J. Am. Chem. Soc.* **2006**, *128*, 4872.
(33) Fukuda, K.; Nakai, I.; Ebina, Y.; Ma, R.; Sasaki, T. *Inorg. Chem.* **2007**, *46*, 4787.
(34) Sakai, N.; Ebina, Y.; Takada, K.; Sasaki, T. *J. Am. Chem. Soc.* **2004**, *126*, 5851.
(35) Wang, Y.; Gao, H. *J. Solid State Chem.* **2006**, *179*, 1870.
(36) Ghosh, P.; Sadhu, S.; Patra, A. *Phys. Chem. Chem. Phys.* **2006**, *8*, 3342.

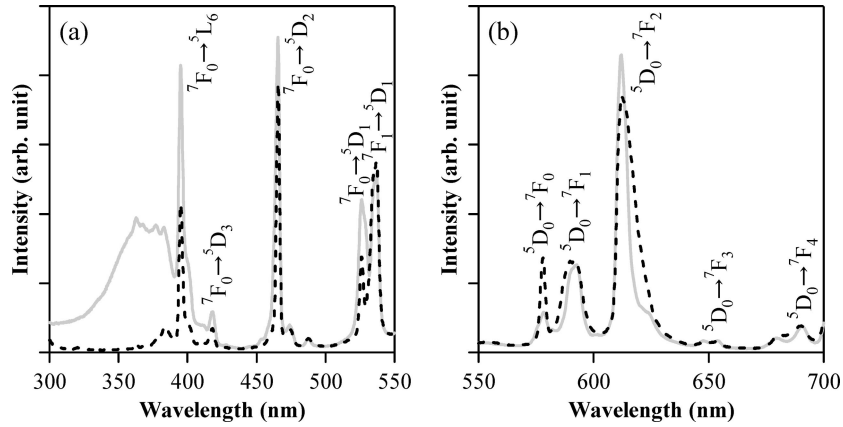

Figure 8. Photoluminescence (a) excitation and (b) emission spectra of bulk precursors $KLa_{0.90}Eu_{0.05}Nb_2O_7$ (gray solid line) and $H_{0.98}K_{0.08}La_{0.90}Eu_{0.05}Nb_2O_7 \cdot 0.25H_2O$ (black dotted line). The excitation spectra were monitored at 612 nm emission, and the emission spectra were obtained by exiting at 466 nm.

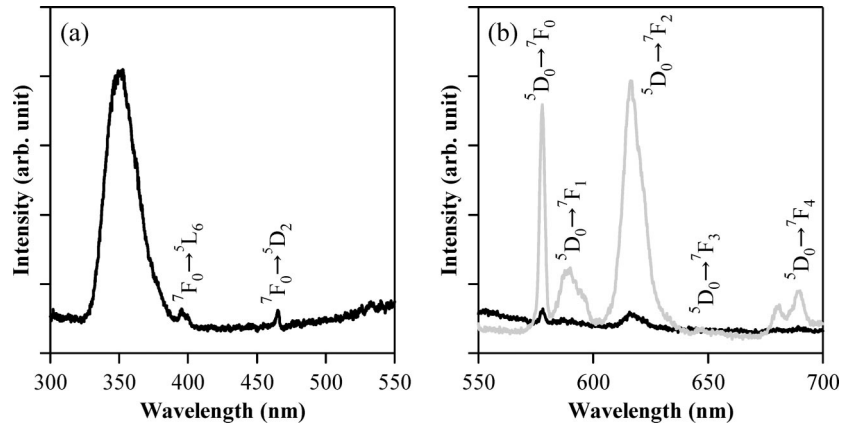

Figure 9. Photoluminescence (a) excitation and (b) emission spectra of $La_{0.90}Eu_{0.05}Nb_2O_7$ nanosheets. The excitation spectra were monitored at 616 nm emission, and the emission spectra were obtained by exiting at 353 (gray line) and 466 nm (black line).

was below 300 nm even though the UV–vis absorption peaks were observed in this range, suggesting the existence of nonradiative relaxation. However, relatively sharp excitation peaks due to the intra-4f transitions of Eu^{3+} were observed for the bulk precursors and $La_{0.90}Eu_{0.05}Nb_2O_7$ nanosheets as generally expected for Eu^{3+}-doped phosphors. In addition, broad excitation bands were observed for both bulk $KLa_{0.90}Eu_{0.05}Nb_2O_7$ and $La_{0.90}Eu_{0.05}Nb_2O_7$ nanosheets around 340–380 nm. These broad excitation bands of $KLa_{0.90}Eu_{0.05}Nb_2O_7$ and $La_{0.90}Eu_{0.05}Nb_2O_7$ nanosheets do not fit to their diffuse reflection spectra (Figure 7). As Kudo proposed for $KLa_{0.98}Eu_{0.02}Nb_2O_7$, these excitation bands might be due to the $O^{2-}-Eu^{3+}$ charge-transfer (CT) transition.[11] The similar CT transition was also observed in the structurally related Eu^{3+}-doped layered perovskites.[37–39] However, this kind of excitation band was quenched in case of $K_{0.08}H_{0.98}La_{0.90}Eu_{0.05}Nb_2O_7 \cdot 0.25H_2O$, and it was likely due to the significant nonradiative relaxation channels provided by the high-energy vibration of species like OH^- and H_2O as observed in other Ln-doped oxides.[40–42]

Furthermore, the excitation from the bulk precursor and nanosheet hosts exhibits slightly different emission peak positions for the $^5D_0 \rightarrow {}^7F_2$ transition of Eu^{3+}. This transition is known to be highly sensitive to the local environment of Eu^{3+}.[43] The emission peak position of the nanosheets seems to be red-shifted by 4 nm with respect to those of the bulk precursors. However, no shift was observed for the nondegenerate $^5D_0 \rightarrow {}^7F_0$ transition peak. On the basis of these observation, the apparent shift observed for the $^5D \rightarrow {}^7F_2$ transition is likely to be due to the different relative intensities of its five Stark components rather than the nephelauxetic effect because of the covalent interaction strength difference between Eu^{3+} activators and the hosts.[44,45]

For efficient photoluminescence by host excitation, the excitation energy has to be transferred within the perovskite layer and interlayer energy migration should be minimized. This propensity has been experimentally observed in structurally related Eu^{3+}-doped layered perovskite systems.[37,46] In this sense, the exfoliated $La_{0.90}Eu_{0.05}Nb_2O_7$ nanosheets

(37) Blasse, G.; Bril, A. *J. Chem. Phys.* **1968**, *48*, 3652.
(38) Kudo, A.; Sakata, T. *J. Phys. Chem.* **1995**, *99*, 15963.
(39) Berdowski, P. A. M.; Blasse, G. *J. Lumin.* **1984**, *29*, 243.
(40) Jeon, S.; Braun, P. V. *Chem. Mater.* **2003**, *15*, 1256.
(41) Di, W.; Wang, X.; Zhu, P.; Chen, B. *J. Solid State Chem.* **2007**, *180*, 467.
(42) Nogami, M.; Umehara, N.; Hayakawa, T. *Phys. Rev. B* **1998**, *58*, 6166.
(43) Carnall, W. T., In *Handbook on the Physics and Chemistry of Rare Earths*; Gschneidner, K. A., Eyring, L., Eds.; North-Holland: Amsterdam, 1979; Vol. 3, p 171.
(44) Jørgensen, C. K., In *Progress in Inorganic Chemistry*; Cotton, F. A., Ed.; Interscience: New York, 1962; Vol. 4, p 73.
(45) Inaguma, Y.; Tsuchiya, T.; Katsumata, T. *J. Solid State Chem.* **2007**, *180*, 1678.
(46) Toda, K.; Kameo, Y.; Ohta, M.; Sato, M. *J. Alloys Compd.* **1995**, *218*, 228.

might have more efficient host to activator energy transfer than the bulk precursors, which have considerable interlayer interactions. Our experimental results are consistent with this expectation. For the bulk precursor phases, direct excitation of Eu^{3+} yielded the most intense photoluminescence emission. In case of $KLa_{0.90}Eu_{0.05}Nb_2O_7$, the direct excitation yielded more than double $^5D_0 \rightarrow {}^7F_2$ transition emission intensity than the host excitation, and only the photoemission via direct 4f transitions of Eu^{3+} was observed in case of $K_{0.08}H_{0.98}La_{0.90}Eu_{0.05}Nb_2O_7 \cdot 0.25H_2O$. On the contrary, for the $La_{0.90}Eu_{0.05}Nb_2O_7$ nanosheet suspension, the host excitation yielded significantly higher emission intensity than the direct excitation of Eu^{3+}. The most intense emission from the $La_{0.90}Eu_{0.05}Nb_2O_7$ nanosheet suspension was observed by exciting at the broad excitation band maximum located at 353 nm. We believe that these differences are largely related to the interlayer interactions of the host structures where more efficient intralayer energy transfer takes place between the nanosheet host and activators by eliminating the interlayer interactions.

The exfoliation of Eu^{3+}-doped layered perovskite phosphors into nanosheets seems like a rational approach to design novel phosphors for solid-state lighting applications. As mentioned in the introduction, phosphors that can efficiently be excited in the near UV range (350–400 nm) are sought for the GaN-based solid-state lighting applications.[12,13] This means that the host excitation is preferred to the direct excitation in case of the Eu^{3+}-activated phosphors because the host excitation band maxima tend to be located closer to this ideal excitation wavelength range than the direct excitation wavelengths of Eu^{3+}. In our experiment, we have shown an example of transformation of a direct excitation (466 nm) dominated phosphor to a host excitation (353 nm) dominated phosphor by means of soft chemical exfoliation of the layered host structure. Studies of higher Eu^{3+} content nanosheets obtained from various layered perovskite precursors are under way to further corroborate the adequacy of our practical phosphor design approach and to search for novel high-performance phosphors.

Conclusion

The Eu^{3+} -activated perovskite nanosheets, $La_{0.90}Eu_{0.05}Nb_2O_7$, were prepared by soft chemical exfoliation of the layered perovskite $K_{1-x}H_xLa_{0.90}Eu_{0.05}Nb_2O_7$. On the contrary to the bulk precursors, photoluminescence emission of $La_{0.90}Eu_{0.05}Nb_2O_7$ nanosheets is dominated by the host excitation rather than the direct excitation of Eu^{3+}. The photoluminescence excitation band maximum of $La_{0.90}Eu_{0.05}Nb_2O_7$ nanosheets is in fact located in the optimum excitation wavelength range for the GaN based solid-state lighting applications.[12,13] It is possible that intralayer Ln activated nanosheets might be, in general, suitable phosphors for solid-state lighting applications because of their morphology and efficient energy transfer from the nanosheet host to Ln. Additionally, a quantum size effect might facilitate to enhance the photoluminescence efficiency in Ln-doped nanosheets like that observed in Ln-doped nanoparticles.[47–49] Furthermore, intralayer activated nanosheets seem like ideal systems to investigate the physics of two-dimensional energy transfer and concentration quenching mechanisms including the percolation model because their faultless two-dimensionality.[46,50,51] To the best of our knowledge, the $La_{0.90}Eu_{0.05}Nb_2O_7$ nanosheet is the first paradigm of such a fascinating intralayer Ln-doped nanosheet phosphor material.

Acknowledgment. We are grateful to Dr. Y. Takahashi for useful discussion on photoluminescence characterizations. We also thank Drs. A. Watanabe and M. Osada for use of their research facilities. This research was financially supported by CREST of the Japan Science and Technology Agency.

CM702552P

(47) Tissue, B. M. *Chem. Mater.* **1998**, *10*, 2837.
(48) Goldburt, E. T.; Kulkarni, B.; Bhargava, R. N.; Taylor, J.; Libera, M. *J. Lumin.* **1997**, *72–4*, 190.
(49) Sharma, P. K.; Jilavi, M. H.; Nass, R.; Schmidt, H. *J. Lumin.* **1999**, *82*, 187.
(50) Van Uitert, L. G.; Linares, R. C.; Soden, R. R.; Ballman, A. A. *J. Chem. Phys.* **1962**, *36*, 702.
(51) Van Uitert, L. G.; Iida, S. *J. Chem. Phys.* **1962**, *37*, 986.